David Tomás Sánchez Martínez
Lourdes García Rodríguez
(coordinadores)

Proceedings of the 7th International Seminar on ORC Power Systems

Editorial Universidad de Sevilla

Proceedings of the 7th International Seminar on

ORC

Power Systems

David Tomás Sánchez Martínez
Lourdes García Rodríguez
(coordinadores)

Proceedings of the 7th International Seminar on

ORC Power Systems

(ORC2023)

4th to 6th
SEPTEMBER
SEVILLE 2023

EDITORIAL UNIVERSIDAD DE SEVILLA

Sevilla, 2024

Colección Actas
Núm.: 91

ISBN 978-84-472-2745-7
DOI: https://dx.doi.org/10.12795/9788447227457

Diseño de cubierta y maquetación: los autores

INDEX OF CONTRIBUTIONS

DOI: https://dx.doi.org/10.12795/9788447227457_26

Investigation of the turbulence level and the vortex shedding in a turbine cascade working with an organic vapor at subsonic Mach numbers

Leander Hake[1,*], Stephan Sundermeier[1], Stefan aus der Wiesche[1],
Camille Matar[2], Paola Cinnella[2], Xavier Gloerfelt[3]

[1] *Muenster University of Applied Sciences, Steinfurt, Germany*
[2] *Sorbonne University, Paris, France*
[3] *ENSAM - Paris Tech, Paris, France*

*Corresponding Author: leander.hake@fh-muenster.de

ABSTRACT

Detailed turbulence and trailing edge vortex shedding measurements employing hot-wire anemometry and numerical simulations using a high-resolution unsteady Reynolds-averaged Navier-Stokes method were conducted for the high subsonic flow of the organic vapor Novec 649 through the VKI turbine cascade at elevated pressure and temperature level. Turbulent spectra downstream and upstream of the cascade were obtained and analyzed. The simulations indicated that acoustics waves (shed shockwaves) and locally supersonic flow occurred at the trailing edge even at a moderate isentropic exit Mach number of 0.7. Strong evidence for that loss-relevant mechanism was found in the hot-wire signals. The vortex shedding frequency depended primarily on the Reynolds number, not the Mach number.

1 INTRODUCTION

Predicting turbulence levels and vortex shedding in turbine cascades is of significant engineering relevance, especially for efficiency calculations. Although powerful computational fluid dynamics (CFD) methods have been developed to simulate the development of turbulence quantities and unsteady flow phenomena in turbomachinery, their accuracy and reliability limits are unclear. That issue is discussed in detail in a corresponding review article by Sieverding and Manna (2020). Especially for organic vapor flows, relatively little is reported regarding the turbulent flow through a turbine cascade and the development of turbulent quantities and transonic vortex shedding. Experimental data are strongly needed to validate numerical methods for these flows.

Sanz et al. (1998) conducted a numerical and experimental investigation of the wake flow downstream of a linear turbine cascade. They studied the turbulent kinetic energy distribution of airflow through the so-called VKI cascade, described by Kiock et al. (1986). In the wake of the blades, relatively high turbulent energy contents were observed. The employed turbulence models (i.e., Spalart-Allmaras and low-Reynolds-number k-ε) could predict the profile pressure distribution and other flow quantities but failed regarding the decay of the turbulent kinetic energy downstream of the cascade. The authors suggested that the periodic vortex shedding caused significant discrepancies between the measured and computed turbulent kinetic energy k from the blunt trailing edge. A steady Reynolds-averaged Navier-Stokes (RANS) approach does inherently not cover such unsteady phenomena, and unsteady RANS (URANS) methods or large-eddy-simulations (LES) or even direct numerical simulations (DNS) are required to resolve these unsteady flow features. Sanz and Scheier (2021) recently reported that the qualitative prediction of secondary flows in a transonic turbine stage was, in their own words, “good,” but their unsteady RANS simulation failed regarding turbulence production and destruction. Significant deviations of more than 100 % were reported between the measured and computed turbulent kinetic energy k at different downstream stations.

That issue also turns the attention to the anisotropy of turbulence in cascade flows. The existence of non-isotropic structures in the wake flow of low-pressure steam turbine airfoils was experimentally indicated by Antos et al. (2018). Several experimental studies performed with air as a working fluid (e.g., Zunino et al. (1987), Gregory-Smith et al. (1988), Dossena et al. (1993), Ames and Plesniak (1995), and Volino et al. (2008)) demonstrated that high turbulent kinetic energy levels can occur in the wake of turbine blades. Melzer and Pullan (2019) presented schlieren pictures demonstrating the existence of acoustic waves (shed shockwaves) at a Mach number of about 0.65 for an idealized trailing edge configuration. It is reasonable to assume that these acoustic waves and their reflections in the cascade contribute significantly to the total turbulent kinetic energy. Since vortex shedding and acoustic wave propagation are coherent fluid motion phenomena, a clear distinction between the true turbulent kinetic energy k and recorded fluctuations is needed for a correct data interpretation and comparison with the outcome of CFD methods.

The present experimental and numerical case study was conducted to provide data for turbulent quantities for a high-subsonic organic vapor flow through a representative turbine cascade. The objective was to increase the understanding of trailing edge flows, acoustic wave propagation, and the production of turbulent kinetic energy. The experimental work is a direct continuation of recent studies regarding losses in organic Rankine cycle (ORC) turbine cascades (i.e., Hake et al. (2022, 2023)). Still, the present investigation focused on turbulence behavior and unsteady flow phenomena. The recently tested hot-wire anemometry described in Hake et al. (2022a) for high-speed organic vapor flows was utilized for this. The present numerical work aimed to study the prediction capabilities of unsteady RANS methods for high-speed organic vapor flows in more detail. Matar et al. (2023) recently demonstrated that steady RANS methods have inherent difficulties in predicting turbulent flow in the wake of a cylinder. In contrast, unsteady RANS (URANS) methods can significantly increase our qualitative understanding of turbulent compressible organic vapor flows.

2 EXPERIMENTAL AND NUMERICAL METHODS

Since reliable literature data (i.e., Sanz et al. (1998) and Melzer and Pullan (2019)) for air are available at a Mach number level of about 0.65, this study employed the same turbine cascade as Sanz et al. (1998) and considered a similar exit Mach number. Although the present study considered only high-subsonic flow and not supersonic flow, the detailed assessment of RANS methods for predicting compressible turbulence production and decay in organic vapors is an essential starting point. In this section, the experimental and numerical methods are briefly explained. Further information can be found in Hake et al. (2022, 2022a, 2023), aus der Wiesche (2023), and Matar et al. (2023).

2.1 Experimental Setup and Procedure

The measurements were performed using the closed-loop organic vapor wind tunnel (CLOWT) at Muenster University of Applied Sciences, shown in Figure 1. The non-toxic organic vapor Novec 649 by 3M was selected as a testing fluid. Its thermodynamic behavior represents working fluids for ORC power systems, and some general thermodynamic properties are listed in Table 1. The nominal experimental stagnation conditions (as obtained by total pressure and temperature measurements in the settling chamber of the wind tunnel), including the compressibility factor Z, isentropic exponent γ, and the fundamental derivative of gas dynamics Γ (calculated using REFPROP), are listed in Table 2.

Table 1: Thermodynamic properties of Novec 649 (after REFPROP by NIST)

Chemical Formula	Molecular Mass	Critical Pressure	Critical Temperature
$CF_3CF_2C(O)CF(CF_3)_2$	316 g/mol	18.8 bar	442 K

Table 2: Nominal stagnation conditions for the experimental study with Novec 649

Pressure p_o	Temperature T_o	Compressibility Factor Z	Isentropic Exponent γ	Fundamental Derivative Γ
2.30 bar	373 K	0.914	1.046	0.946

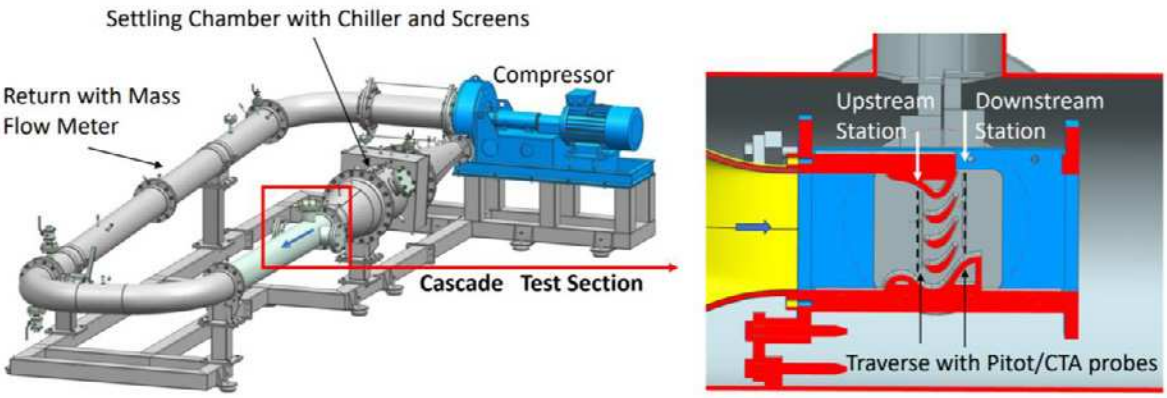

Figure 1: Wind tunnel facility CLOWT with main components and details of the cascade test section.

The airfoil profile for the cascade, established by three full blades and two half-profile pieces, see Figure 1, was the same as described by Kiock et al. (1986) and Sanz et al. (1998). Data for the test cascade are listed in Table 3. The actual roughness level was comparable with aged airfoils. At the upstream and downstream stations, see Figure 1, hot-wire probes in the constant-temperature mode (CTA) and Pitot probes were traversed in the *y*-direction. The minimal normalized distance *x/c* between the trailing edge and the probe head (i.e., the downstream station 2) was similar to Sanz et al. (1998) namely $x/c = 0.04$. In addition to the hot-wire and Pitot probe measurements, static pressure measurements were conducted using twenty wall pressure taps at the central blade passage under investigation. Furthermore, the vibration behavior of the downstream CTA probe and its stem was observed using a high-speed camera and optical access to the cascade through a window.

The desired exit Mach number M_2 was controlled by the variable wind tunnel compressor running speed, which was adjustable via the electric engine frequency. The maximum exit Mach number and Reynolds number were $M_2 = 0.70$ and $Re_2 = 3.2 \times 10^6$, respectively. The temperature drift rate during a single CTA sampling time (5 up to 10 s) at a single traverse location was only 10^{-3} K/s leading to nearly constant total temperature conditions. However, absolute stagnation temperature deviations from the nominal conditions listed in Table 2 of about $\Delta T_o = \pm 2$ K occurred during the total campaign. 161

Table 3: Cascade data for the present case study

Quantity	Symbol	Value
Spacing (blade pitch)	t	22.0 mm
Chord	c	30.5 mm
Axial chord	b	25.0 mm
Throat	o	8.3 mm
Span	H	50.0 mm
Trailing edge thickness	t_{TE}	1.4 mm
Relative airfoil roughness	k_s/c	4×10^{-4}
Nominal inflow/exit angles	β_1 / β_2	30° / 67.8°

The primary investigation tool was the hot-wire anemometry (HWA) in the constant-temperature mode (CTA). Single tungsten wire probes (L-shape probe design with wire diameter $d = 10$ µm and length $l = 4$ mm) were employed as described by Hake et al. (2022a, 2022b). The hot wire probes were aligned normally to the main flow direction in the center line of the cascade. The anemometer was based on a modified electric circuit and amplifier device manufactured by SVMtec (Stuttgart, Germany). The bandwidth was 20 kHz (low-pass filter), and the sampling frequency was 50 kHz. The hot wire signal was digitalized and processed by components manufactured by NI, and the data reduction and post-processing filtering were performed using MATLAB software.

The generalized King equation for the average output electrical voltage signal

$$\bar{E}^2 = A(M, T_o) + B(M, T_o)(\rho u)^{1/2} \qquad \text{(with } E = \bar{E} + E'\text{)} \tag{1}$$

has proven its reliability (Hake et al. (2022a, 2022b), de Souza and Tavoularis (1998)). The coefficients A and B in Equation (1) depend on the Mach number M and total temperature T_o. The total temperature was fixed during the experiments, and only the Mach number dependency remained. During the calibration, the mass flux ρu was varied for a given Mach number level M, and the electrical voltage output E was recorded. The calibration measurements were executed at the upstream station (for the low M levels) and downstream station (for the high M levels) of the cascade. For the calibration, the probes were placed in the center of the blade passage where nearly uniform flow conditions existed. The outcome of a previous Pitot probe test combined with static pressure taps was used to obtain the required reference calibration velocities at these locations.

The above *in situ* calibration approach avoided issues with mounting and demounting probes during the experimental campaign. However, an independent calibration study using different wire dimensions was necessary to derive the required correction scheme for obtaining quantitative results. The signal attenuation due to the finite wire length l compared to the turbulent macro length Λ and the cut-off frequency limitation made appropriate correction schemes necessary (Hake et al. (2022b). Two different correction schemes were applied, namely (i) the wire length attenuation correction proposed by Dryden et al. (1937) resting on the integral length scale Λ obtained by the autocorrelation function and (ii) the Wyngaard (1968) correction scheme assuming local isotropy. The correction due to the finite bandwidth was done by assuming a Lorentzian profile for the spectra resting on the actual macro length scale Λ (Hinze (1975)) and calculating the suppressed spectral contribution due to the actual cut-off frequency by numerical integration.

Additional wire vibrations (natural frequencies of the probe device, including wire and the stem) occurred due to the high dynamic loads in high-speed flows. The corresponding natural frequencies were calculated using relations from structural dynamics (see, for instance, Szabo (2001)). Stem vibrations could be identified optically by the high-speed camera approach.

The fluctuating part E' of CTA signals depends on density, velocity, and temperature or pressure fluctuations (de Souza and Tavoularis (1998)):

$$\frac{E'}{\bar{E}} = \left(S_u + (\gamma - 1)M^2 S_\rho\right)\frac{u'}{\bar{u}} + S_\rho \frac{p'}{\bar{p}} + \left(S_T - (1 - \frac{\gamma-1}{2}M^2)S_\rho\right)\frac{T_o'}{T_o} \qquad (2)$$ 162

The high Reynolds number and wire overheat ratio led to the identity of the sensitivity coefficients S_ρ and S_u for density and velocity, as demonstrated by Hake et al. (2022a). Hence, only mass flux $(\rho u)'$ and pressure p' fluctuations contributed to E' for a fixed total temperature T_o. As de Souza and Tavoularis (1998) discussed, the additional pressure fluctuation contribution can be substantial. The existence of acoustic waves increases the fluctuation level of the electrical HWA signal, and it is impossible to distinguish the fluctuation modes in a compressible flow employing only HWA. In the present study, a pseudo-turbulence intensity Tu^* and a pseudo-turbulent kinetic energy k^* was obtained resting on the measured fluctuating and average output signals. In the case of vanishing pressure fluctuations, these quantities would be identical to the usual turbulence intensity Tu and turbulent kinetic energy k. However, in the case of acoustic waves with their coherent fluid motion contributions, Tu and Tu^* systematically differ (with $Tu^* > Tu$). That was the case for the present investigation at higher Mach numbers. Hence, Tu's proper turbulence intensity was estimated by filtering out the coherent contributions to the total recorded power density spectrum. It is important to note that the systematic difference between Tu and Tu^* is a consequence of Equation (2) and is not directly related to non-ideal gas dynamics.

2.2 Computational Fluid Dynamics Method

Two-dimensional compressible steady and unsteady RANS simulations were carried out using the in-house MUSICAA finite-difference solver. The inviscid fluxes were discretized by means of 4th-order centered differences, whereas the 2nd-order was used for viscous fluxes. The scheme was supplemented with a 4th-order selective filter to eliminate grid-to-grid oscillations and a low-order shock-capturing term activated locally by combining Jameson's (2017) shock sensor and the Ducros et al (1999) dilatation/vorticity sensor. A four-stage Runge-Kutta algorithm was used for time integration, and high-order implicit residual smoothing (Cinnella et al. (2015)) was applied to relax stability constraints on the time step. A CFL number of 0.5 was fixed throughout the computational domain to decrease the time-to-convergence of the steady RANS solutions, while in the URANS computations, the time step was fixed and the maximum CFL number reached in the domain was 5. Turbulence modeling was performed through the Spalart-Allmaras (SA) eddy viscosity model, modified by Crivellini et al.. The SA model does not explicitly compute the turbulence kinetic energy k. However, we used the same relation ($k = \mu_t \Omega/(\rho (C_\mu)^{1/2})$) as used by Sanz et al. (1998) to obtain an approximation for k. The Reynolds stress was then computed using the linear Boussinesq hypothesis. Because the Reynolds number level was high, the flow was fully turbulent from the front stagnation point. Since the experiments were carried out with rough blades, see Table 3, the existence of a turbulent boundary layer flow seemed to be reasonable.

The behavior of the dense gas was modeled by the equation of state of Peng-Robinson improved by Stryjek and Vera (Stryjek et al. (1986)), along with a power-law approximation of the specific heat at constant volume in the dilute gas limit. Dynamic viscosity and thermal conductivity coefficients were computed using the Chung-Lee-Starling models (Chung et al. (1988)). At the inlet, conservation of Riemann invariants and total temperature and pressure was imposed, while a simple extrapolation was performed at the outlet where the static pressure was imposed. The periodic flow was assumed in the pitch-wise direction, so only one blade passage of an infinite cascade was simulated. The computational domain extended from −2.5 to 2 projected chords in the streamwise direction. The blade passage was discretized using a multi-block structured curvilinear mesh. First, an O-block was extrapolated from the blade surface with a fixed cell growth rate of 1.05 over 150 points and then connected to H-blocks, see Figure 2 (left). Cell clustering was performed in the TE region to increase the spatial resolution of the unsteady wake, amounting to a total of 165 000 points, see Figure 2 (right), which was found to be appropriate after a grid-convergence study.

Figure 3 shows the computed isentropic Mach number distribution for Novec 649 at an exit Mach number of M_2 = 0.70 (as in the present experiments) and air at M_2 = 0.64 (as in Sanz et al. (1998)). While both RANS and URANS show similar overall trends, the trailing edge region exhibited some local differences. The qualitative agreement with the experimental data from Sanz et al. (1998) was reasonable, with maximum deviations of 7 % and 9 % located at $s/c \approx 0.4$, 0.2 on the suction and pressure sides, respectively. 163

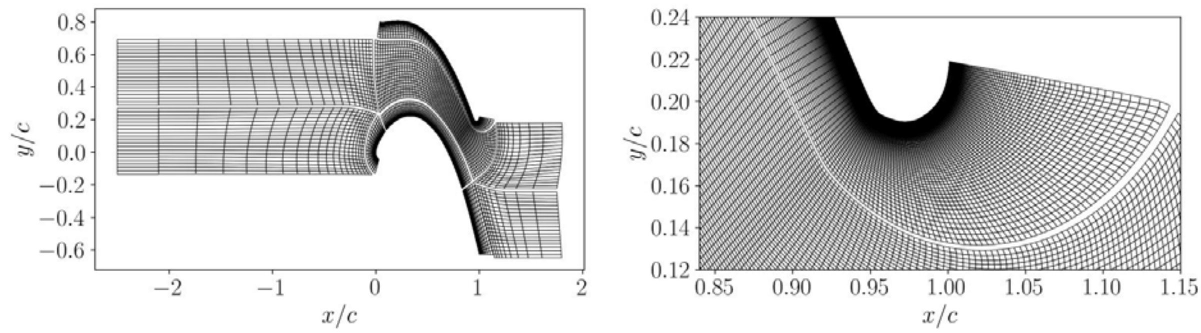

Figure 2: Computational mesh with shown every fifth line (left) and trailing edge details (right)

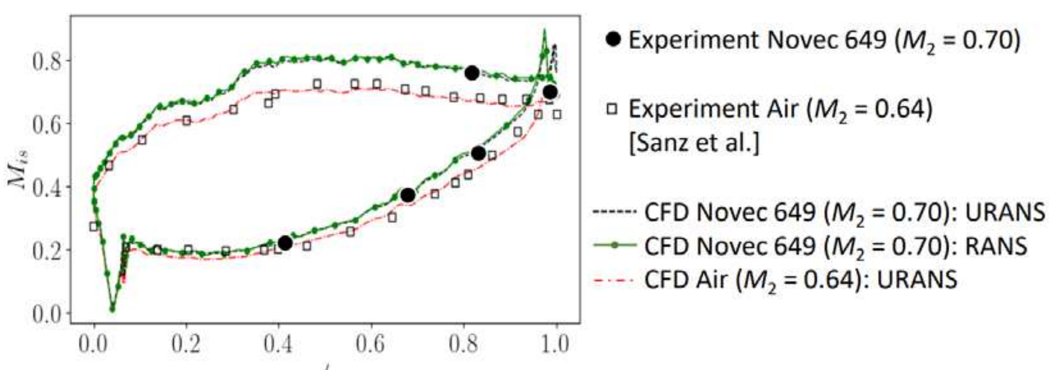

Figure 3: Computed and experimentally determined isotropic profile Mach number distribution

3 RESULTS AND DISCUSSION

3.1 Inflow Conditions

The measured inflow (pseudo) turbulence intensity $Tu*$ (see Section 2.2) against the inlet and exit Mach numbers M_1 and M_2 are plotted in Figure 4 (left). The data point sets correspond to the two different HWA data correction schemes (i) and (ii). However, the same qualitative behavior of the measured turbulence intensity $Tu*$ resulted. For low Mach numbers, the inflow fluctuation level increased linearly, but an extreme rise in the turbulence intensity $Tu*$ can be seen for an exit Mach number M_2 = 0.70. Filtering out the contributions assumed to be caused by coherent fluctuations, the red symbols denoted by "corrected" can be derived in Figure 4 (left). These data followed a linear trend and might be assumed as the proper inflow turbulence intensity Tu. The inflow power density spectra shown in Figure 4 (right) demonstrate the existence of additional natural frequency contributions. The location of the measuring point was close to the blade stagnation point (see inset of Figure 4). The spectrum for the higher exit Mach number did not exhibit an amplitude decrease with frequency. This is indicating a loss of isotropy due to the emission of pressure waves affecting the HWA signal, see Equation (2).

3.2 Trailing Edge Vortex-Shedding

The trailing edge vortex shedding was investigated using the power spectra obtained at the downstream station. Samples of spectra obtained in the wake of the trailing edge are shown in Figure 5. The shedding frequency 1x and their double 2x (CTA is not sensitive in flow direction) can be identified clearly in the power spectra for M_2 = 0.13. In the case of higher Mach numbers, the high dynamic loads caused significant vibrations of the wire and the probe stem, adding several artificial peaks to the power spectrum (noticeably also in the inflow spectra shown in Figure 4). These resonances correspond to the natural frequencies of the mechanical systems. Whereas in the case of the low Mach number, the spectrum decreases roughly with an exponent of −5/3, indicating isotropy, a nearly constant spectrum resulted for M_2 = 0.70, indicating a loss of isotropy as observed by Antos et al. (2018).

The vortex-shedding frequency f can be expressed by a non-dimensional Strouhal number $St = f t_{TE}/\bar{u}_2$ defined by the trailing edge thickness t_{TE} and the average exit velocity. The vortex shedding 164
Strouhal numbers St against exit Reynolds and Mach numbers are shown in Figure 6. The data obtained by HWA for the organic vapor Novec 649 are compared with literature data obtained by Sieverding and Heinemann (1990) for air for the same cascade at different test facilities (denoted as VKI and DFVLR in Figure 6). The Reynolds number level was higher for the organic vapor than for the same Mach number in air. Hence, the range of Re_2 was larger for Novec 649, but the same range for M_2 was achieved. Plotting the Strouhal number against the Reynolds number (Figure 6, left) led roughly to an agreement with both literature data sets. The deviations at lower Reynolds numbers can be attributed to the different trailing edge shapes and turbulence conditions in the involved test facilities VKI and DFVLR. However, a significant deviation can be observed between the data set DFVLR and the Novec 649 and VKI data if one plots the Strouhal number against the exit Mach number (Figure 6, right).

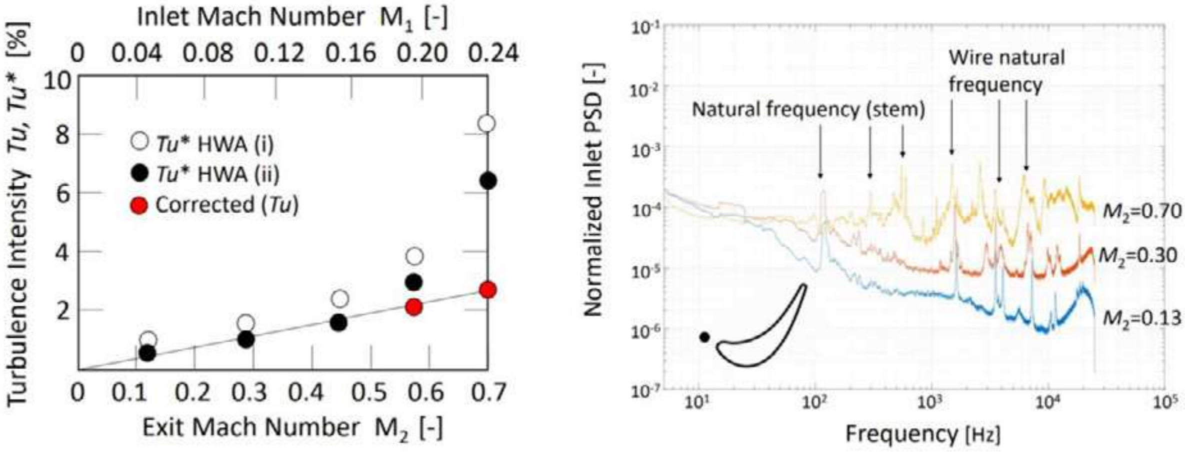

Figure 4: Inflow turbulence intensity Tu against M_2 (left) and inflow power spectra (right).

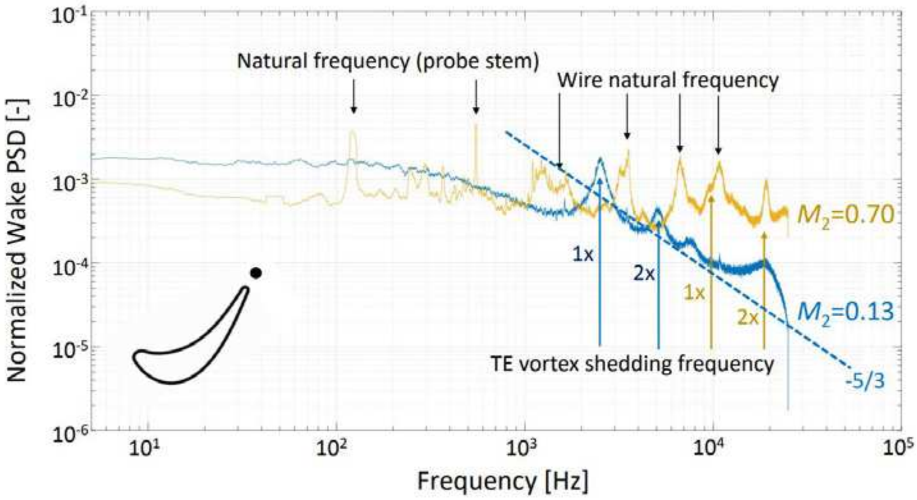

Figure 5: Power spectra obtained in the blade wake region for $M_2 = 0.13$ and $M_2 = 0.70$.

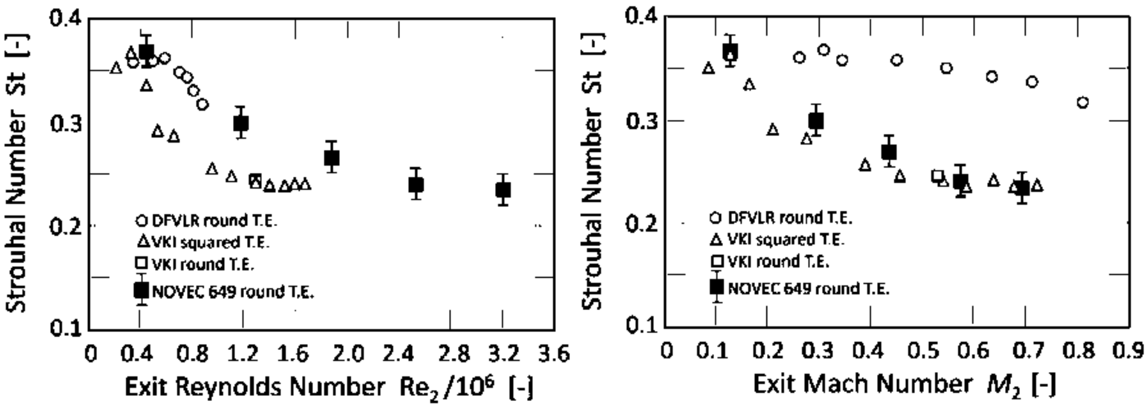

Figure 6: Vortex shedding Strouhal number against Re (left) and against Mach number (right).

Then, two clearly different branches of Strouhal numbers resulted. This can be interpreted as evidence for the hypothesis of Sieverding and Heinemann (1990) that the Reynolds number and the boundary layer flow are the primary quantities for vortex shedding and not the compressibility expressed by the Mach number. The new Novec 649 measurements supported roughly this hypothesis.

Acoustic waves can also interact with the vortex street, and for higher Mach numbers, a complex flow and loss behavior results (Melzer and Pullan (2021)). The URANS study can illustrate this. Figure 7 (left) shows a numerical-schlieren picture for Novec 649 at $M_2 = 0.70$, demonstrating the existence of vortex shedding and acoustics waves. Samples of numerically obtained power spectra are shown in Figure 7 (right).

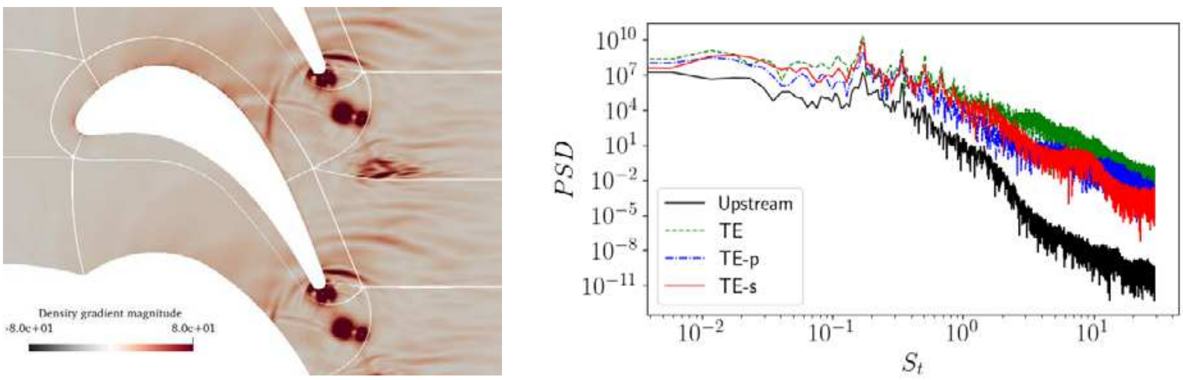

Figure 7: URANS simulations of the vortex street (left) and power spectra (right) for $M_2 = 0.70$.

In the computations, the pressure power density spectra (PSD) are computed at an upstream position of the blade (Upstream), just downstream of the trailing edge (TE), near the TE on the pressure (TE-p) and suction (TE-s) sides, respectively. Hence, the upstream spectrum should feature only pressure fluctuations caused by the upstream traveling acoustic waves, while the TE PSDs also capture the vortex shedding characteristic frequency. The computed peak Strouhal number was $St = 0.17$, identical at all positions. Its value deviated from the measured values ($St \approx 0.23$). That might indicate a shortcoming of the URANS method: as the turbulence kinetic energy content is not well resolved (see also below).

3.3 Cascade Exit Wake Flow Results

Wake flow results against the normalized traverse coordinate y/t are plotted in Figure 8. The flow data were obtained at the downstream station close to the blade trailing edge. In addition to the new Novec 649 data, the literature data for air reported by Sanz et al. (1998) are shown (in red color).

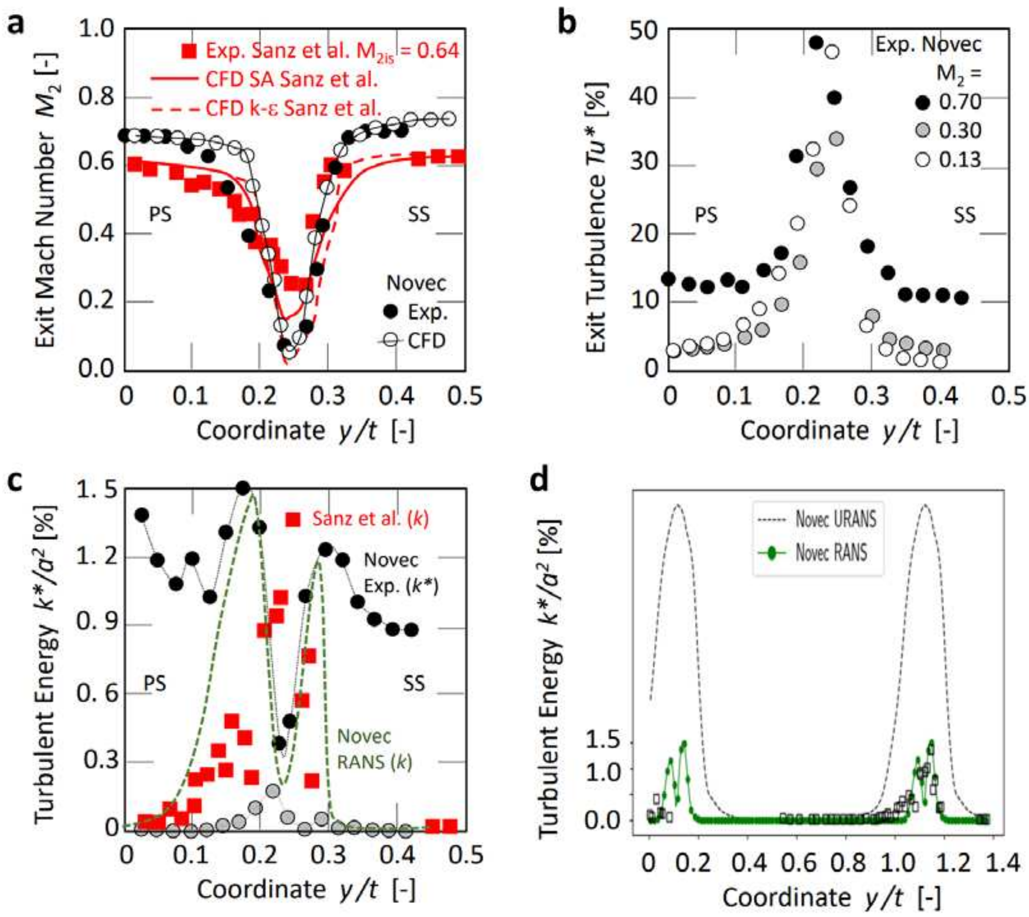

Figure 8: Wake flow profiles: **a** Mach number, **b** pseudo turbulence intensity Tu^*, **c** normalized (pseudo)-turbulent kinetic energy k^*/a^2, **d** computed (pseudo)-turbulent kinetic energy k^*/a^2

166

The qualitative agreement between experiment and CFD for Novec 649 regarding the exit Mach number M_2 was reasonable, Figure 8.a. The present HWA measurements for the local turbulence intensity Tu^* (Figure 8.b) exhibited the expected behavior: a significant peak at the trailing edge for all Mach numbers existed. The level for Tu^* was quite high in the wake, but it should be kept in mind that coherent fluid motion (vortex shedding and acoustic waves) contributed to the total recorded fluctuations signals. That can be seen clearly in the comparison of the normalized turbulent kinetic energy k^*/a^2 (Figure 8.c). Here, the measured turbulent kinetic energy k^* was normalized by the square of the stagnation speed of sound a. The hot-wire probe enabled a resolution of the local fluctuation minimum at the trailing edge. At the suction and the pressure side of the airfoil, the turbulent kinetic energy reached local maxima in the turbulent boundary layers, but outside of the boundary layers, the measured level for Novec 649 was very high in the case of the higher Mach number $M_2 = 0.70$. The asymmetry regarding the pressure and suction side can be attributed to shockwave reflections that are only present on the pressure side (PS) of the trailing edge, with the reflection occurring from the suction surface (SS) of the adjacent blade (Melzer and Pullan (2019)). Since acoustic waves did not occur at low Mach number levels, the Novec 649 data for $M_2 = 0.3$ did not exhibit such a high fluctuation energy level in the passages away from the blades. That observation indicated that outside of the boundary layer and wake domain, the hot-wire signals must be corrected regarding the acoustic wave contributions. Regarding the turbulent kinetic energy level, Figure 8.d, the steady RANS predictions were in much better agreement with the present measurements than the URANS. URANS largely overpredicted the peak due to the large velocity fluctuations caused by the passage of each vortex, while the overall amplitude found in the RANS solution was in good agreement with the present measurements, Figure 8.d. This is essentially due to the different mean recirculating flow sizes behind the TE, which was much smaller in URANS. This tendency was already observed in the case of the wake behind a circular cylinder (Matar et al. (2023)), and is shown here in Figure 9. While two mean counter-rotating vortices extending over more than 5 % of the axial chord were observed in the RANS computations, the recirculation region only covered 2 % in the URANS and was asymmetric.

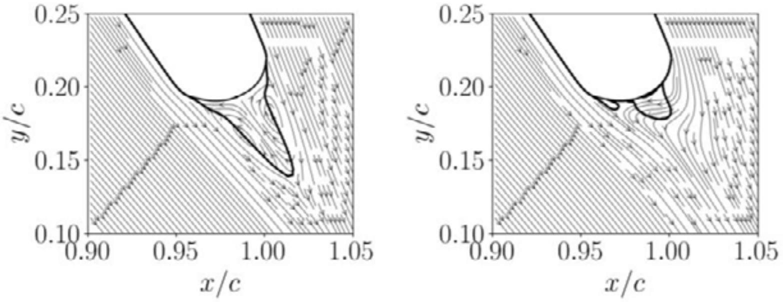

Figure 9: Streamlines (arrows) and null main flow direction velocity component iso-contour (thick black contour) indicating extent of mean recirculation region from RANS (left) and URANS (right)

167

4 CONCLUSIONS AND OUTLOOK

The main findings of the present experimental and numerical study of the high-subsonic turbulent flow of an organic vapor through a turbine cascade can be summarized as follows:

- Transonic vortex shedding inclusive acoustic waves and a loss of isotropy occurred for exit Mach numbers $M_2 > 0.5$, fully in agreement with the observations in the literature
- Vortex shedding and pressure fluctuations significantly contributed to the turbulence level and hence to the trailing edge losses at exit Mach numbers of about $M_2 = 0.7$
- High-resolution unsteady RANS (URANS) methods can qualitatively predict transient transonic vortex shedding features including acoustic waves, but the absolute levels of turbulent kinetic energy were largely overpredicted by URANS, and RANS led to a better result regarding the predicted turbulent kinetic energy in the wake
- A careful interpretation of fluctuation signals is required for a correct interpretation of hot-wire measurements and numerical simulations

The exploration of large-eddy-simulation (LES) methods for predicting transonic vortex shedding is the subject of ongoing research.

REFERENCES

aus der Wiesche, S., 2023, Experimental Investigation Techniques for Non-Ideal Compressible Fluid Dynamics, *Int. J. Turbomach. Propuls. Power*, vol. 8(2), p. 11

Ames, F. E., Plesniak, M. W., 1995, The influence of large scale, high intensity turbulence on vane aerodynamic losses, wake growth, and the exit turbulence parameters, *Proc. ASME Turbo Expo*, 5 – 8 June 1995, Houston, Texas, paper 95-GT-290

Antos, P., Uruba, V., Jonas, P., Prochazka, P., Skala, V., Hoznedl, M., Sedlak, K., 2018, Measurement of turbulence in LP part of the 1090 MW steam turbine, *Proceedings XXIV Biennial Symposium on Measuring Techniques in Turbomachinery*, 29 – 31 August 2018, Prague, Czech Republic, paper MTT2418A31

Chung, T., Ajlan, M., Lee, L., Starling, K., 1988, Generalized multiparameter correlation for nonpolar and polar fluid transport properties, *Ind. Eng. Chem. Res*., vol. 27, no. 4, p.671–679

Cinnella, P., et al., 2015, Recent Progress in High-Order Residual-Based Compact Schemes for Compressible Flow Simulations: Toward Scale-Resolving Simulations and Complex Geometries, in: *Notes on Numerical Fluid Mechanics and Multidisciplinary Design Volume 128*, pp 397-421, Springer, Berlin,

de Souza, F., Tavoularis, S., 1998, Hot-Wire Response in High-Subsonic Flow, *Proc. 37th AIAA Aerospace Sciences Meeting and Exhibition*, January 11-14, 1999, Reno, NV, paper AIAA 99-0310

Dossena, V., Perdichizzi, A., Ubaldi, M., Zunino, 1993, Turbulence measurements downstream of a turbine cascade at different incidence angles and pitch-chord ratios, *Proc. ASME Turbo Expo*, 24 – 27 May 1993, Cincinnati, Ohio, paper 93-GT-52

Dryden, H. L., Schubauer, G. B., Mock, W. C., Skramstad, H. K., 1937, Measurements of Intensity and Scale of Wind-Tunnel Turbulence and Their Relation to the Critical Reynolds Number of Spheres, NACA No. 581

Ducros, F., Ferrand, V., Nicoud, F., Weber, C., Darracq, D., Gacherieu, C., Poinsot, T., 1999, Large-Eddy Simulation of the shock/turbulence interaction, *JCP*, vol. 152(1), pp. 517–549

Gregory-Smith, D. R., Walsh, J. A., Graves, C. P., Fulton, K. P., 1988, Turbulence Measurements and Secondary Flows in a Turbine Rotor Cascade, *ASME J. Turbomachinery*, vol. 110, pp. 479-485

Hake, L., Reinker, F., Wagner, R., aus der Wiesche, S., Schatz, M., 2022, The Profile Loss of Additive Manufactured Blades for Organic Rankine Cycle Turbines, *Int. J. Turbomach. Propuls. Power*, vol. 7(1), 11

Hake, L., Sundermeier, S., Cakievski, L., Bäumer, J., aus der Wiesche, S., Matar, C., Cinnella, P., Gloerfelt, X., (2022a), Hot-Wire Anemometry in High Subsonic Organic Vapor Flows, *Proc. ASME Turbo Expo*, June 2022, Rotterdam, The Netherlands, paper GT2022-81689

Hake, L., Sundermeier, S., aus der Wiesche, S., Bienner, A., Gloerfelt, X., Matar, C., Cinnella, P., 2022b, CFD-supported data reduction of hot-wire anemometry signals for compressible organic vapor flows. *Proc. XXVI Biennial Symposium on Measuring Techniques in Turbomachinery*, September 2022, Pisa, Italy

Hake, L., Sundermeier, S., aus der Wiesche, S., 2023, Profile Loss Prediction for Organic Rankine Cycle Turbines: An Experimental Case Study, *Proc. 15th European Turbomachinery Conference*, 24 – 28 April 2023, Budapest, Hungary

Hinze, J. O., 1975, *Turbulence*, 2nd edition, McGraw-Hill, New York

Jameson, A., 2017, The origins and further development of the Jameson-Schmidt-Turkel (JST) scheme. AIAA J., vol. 55(5)

Kiock, R., Lehthaus, F., Baines, N. C., Sieverding, C. H., 1986, The Transonic Flow Through a Plane Turbine Cascade as Measured in Four European Wind Tunnels, *ASME J. Eng. Gas Turb. Power*, vol. 108, 277-284

Matar, C., Cinnella, P., Gloerfelt, X., Reinker, F., aus der Wiesche, S., 2023, Investigation of non-ideal gas flows around a circular cylinder, *Energy*, vol. 268, p. 126563

Melzer, A. P., Pullan, G., 2019, The Role of Vortex Shedding in the Trailing Edge Loss of Transonic Turbine Blades, *ASME J. Turbomachinery*, vol. 141(4), paper 041001

Sanz, W., Gehrer, A., Woisetschläger, J., Forstner, M., Artner, W., Jericha, H., 1998, Numerical and experimental investigation of the wake flow downstream of a linear turbine cascade, *Proc. ASME Turbo Expo*, 2 – 5 June 1998, Stockholm, Sweden, paper 98-GT-246

Sanz, W., Scheier, D., 2021, Unsteady Simulation of a Transonic Turbine Stage with Focus on Turbulence Prediction, *Int. J. Turbomach. Propuls. Power*, vol. 6, p. 36

Sieverding, C. H., Heinemann, H., 1990, The Influence of Boundary Layer State on Vortex Shedding From Flat Plates and Turbine Cascades, *ASME J. Turbomachinery*, vol. 112, pp. 181-187

Sieverding, C. H., Manna, M., 2020, A Review on Turbine Trailing Edge Flow, *Int. J. Turbomach. Propuls. Power*, vol. 5(2), p. 10

Stryjek, R., Vera, J. H., 1986, PRSV: An improved Peng–Robinson equation of state for pure compounds and mixtures, *The Canadian Journal of Chemical Engineering*, vol. 64, no. 2, p. 323–333

Szabo, I., 2001, *Höhere technische Mechanik*, Springer, Berlin

Volino, R. J., Kartuzova, O., Ibrahim, M. B., 2008, Experimental and computational investigations of separation and transition on a highly loaded low-pressure turbine airfoil: Part 2 – high freestream turbulence intensity, *Proc. IMECE*, October 31 – November 6, 2008, Boston, Massachusetts, paper IMECE2008-68776

Wyngaard, J. C., 1968, Measurement of small-scale turbulence structure with hot wires, *J. Scientific Instruments*, vol. 1, pp. 1105-1108

Zunino, P., Ubaldi, M., Satta, A., 1987, Measurements of secondary flows and turbulence in a turbine cascade passage, *Proc. ASME Turbo Expo*, May 31 – June 4, 1987, Anaheim, California, paper 87-GT-132

ACKNOWLEDGEMENT

This study was conducted within the Franco-German research project REGAL-ORC funded by ANR and DFG.

This book contains the compilation of works contributed to the *7th International Seminar on Organic Rankine Cycle Power Systems* (ORC 2023), held in Seville between the 4th and 6th of September 2023. The event was hosted by Universidad de Sevilla on behalf of the Knowledge Centre on Organic Rankine Cycle Technology (KCORC), incorporated in The Netherlands.

The ORC conference, organized biennially, stems as the only conference that is specific to ORC technology, therefore gathering a diverse community whose affiliation spans across all the interested stakeholders, not only in this particular technology but also and in a broader context, in the energy transition. Original equipment manufacturers, professional associations, end-users, investors, policy makers, academics, scientists feel at home at ORC 2023.

The almost 100 proceedings in this book cover a wide variety of topics, from fundamentals to system integration through component design, accounting for thermodynamic performance as well as component design. In addition to this, and as a new track in 2023, works on heat pump technology were also accepted in order to raise awareness of the strong ties between both technologies, specifically in energy storage applications.

This book provides an excellent overview of the current maturity of power systems based on Organic Rankine Cycle technology for applications as diverse as geothermal and waste heat recovery in industry or downstream of other prime movers (e.g., marine applications). It is also an excellent source of information to understand the current challenges faced by the technology, stemming from a very competitive market and increasingly stringent environmental regulations.

The organizers of ORC 2023 hope that the reader finds this work as exciting as the attendees to the conference and, maybe, make the decision to join the 8th edition to the conference in 2025.

KCORC
KNOWLEDGE CENTER
ORGANIC RANKINE CYCLE

eus EDITORIAL
UNIVERSIDAD DE SEVILLA